electronics

MDPI

Article

A CC-Type IPT System Based on S/S/N Three-Coil Structure to Realize Low-Cost and Compact Receiver

Lin Yang [1,2,3], Shuai Shao [1,2,3,*], Haiting Wu [1,2,3], Shuai Jiang [1,2,3] and Li Zhang [1,2,3,*]

[1] College of Electronic and Electrical Engineering, Henan Normal University, Xinxiang 453007, China
[2] Henan Key Laboratory of Optoelectronic Sensing Integrated Application, Henan Normal University, Xinxiang 453007, China
[3] Academician Workstation of Electromagnetic Wave Engineering of Henan Province, Henan Normal University, Xinxiang 453007, China
* Correspondence: 2122283034@stu.htu.edu.cn (S.S.); zhangli2019@htu.edu.cn (L.Z.)

Abstract: The characteristics of load-independent constant current (CC) output and zero phase angle (ZPA) operation are required in many scenarios of inductive power transfer (IPT) applications. However, the existing topologies with CC output characteristics usually need to introduce additional compensation components on the receiving side to compensate for reactive power and achieve the preset function. This not only increases the occupied space of the receiving side, but also increases the cost and weight. Therefore, this study proposes a new IPT system based on an S/S/N three-coil structure. The proposed system can achieve the CC output function and an operation nearly ZPA and zero-voltage switching (ZVS) through flexible parameter design. Moreover, there are no compensation components on the receiving side of the proposed system, which guarantees a low-cost, lightweight, and compact receiver. Firstly, a comprehensive analysis of the proposed S/S/N three-coil structure IPT system that implements CC output characteristics and ZPA operation is provided. Then, the conditions for realizing ZVS are discussed in terms of parameter design and the sensitivity of CC output characteristics to the changes in compensation capacitance parameters. Furthermore, the proposed S/S/N three-coil structure IPT system is compared with previous related studies to reflect its advantages. Finally, the correctness of the theory is verified by simulation and experiment.

Keywords: inductive power transfer; S/S/N; constant current output; zero phase angle; zero-voltage switching

Citation: Yang, L.; Shao, S.; Wu, H.; Jiang, S.; Zhang, L. A CC-Type IPT System Based on S/S/N Three-Coil Structure to Realize Low-Cost and Compact Receiver. *Electronics* **2023**, *12*, 463. https://doi.org/10.3390/electronics12020463

Academic Editors: Sohail Mumtaz, Syed Muzahir Abbas and Pradeep Lamichhane

Received: 28 November 2022
Revised: 12 January 2023
Accepted: 14 January 2023
Published: 16 January 2023

1. Introduction

Wireless power transfer (WPT) enables energy transfer through electromagnetic coupling between terminal coils [1]. In recent years, WPT has attracted much attention due to its safety, flexibility, electrical isolation, and reliability advantages [2]. These advantages make WPT widely used in various industrial fields, such as electric vehicles [3,4], consumer electronics [5,6], biomedical implants [7,8], and unmanned aerial vehicles [9,10], and so on.

In previous studies, the constant voltage output characteristic was mostly taken as the research object of researchers [11–13]. However, the constant current (CC) output characteristic was preferable in some specific IPT applications, such as CC sources for LEDs driving [14,15]. The authors in [16,17] respectively proposed the CC-Type IPT systems based on LC/CC compensation and LCL/P compensation. However, a bulky filter inductor is required at the rear stage of the rectifier in these two systems, which undoubtedly increases the size, cost, and weight of the receiver of the IPT system. The S/S/P compensated three-coil IPT system proposed in [18] faces the same structural problem as the systems in [16,17]. The authors in [19] proposed a dual-LCC IPT system to achieve CC output characteristics. Although this IPT system has no bulky filter inductor on the receiving side, too many compensation components are introduced, which increases the weight, loss, and overall cost. In [20], the authors proposed an LC/CL IPT system to achieve CC

output characteristics. This system effectively reduces the number of system compensation components. Unfortunately, there is a series of compensation inductance on the receiving side. It is well known that the compensation inductor has a higher cost and weight than the compensation capacitor. Therefore, the compact and low-cost receiver is still not guaranteed. Furthermore, the authors proposed the LC/S IPT system in [21], which further reduces the system compensation components and can realize good CC output function and ZPA operation. Nevertheless, there is still one compensation capacitor on the receiving side, which increases the weight and cost of the receiving side to a certain extent. The SS IPT system proposed in [22] is currently recognized as the simplest CC-Type IPT system. However, the same as with the LC/S IPT system proposed in [21], an inevitable compensation capacitor exists on the receiving side of the SS IPT system. To further optimize the receiving side of the IPT system in terms of low cost and compactness, a new IPT system based on an S/S/N three-coil structure is proposed in this study, and a comprehensive analysis and the design process are provided. Compared with the SS IPT system with compensation capacitance at the receiving side, the proposed S/S/N three-coil structure IPT system can also achieve CC output characteristics and ZPA operation. The difference is that this system has a three-coil structure, and the relay and transmitting coils are placed coaxially and in coplanarity. Notably, there are no compensation components at the receiving side of the system. A low-cost, lightweight, and compact receiver is ensured, which is crucial in some special wireless charging applications, for example, implantable medical devices (IMDs) and unmanned aerial vehicles (UAVs) with strict volume and weight requirements, and others.

Specifically, Section 2 provides a fundamental principle analysis of the proposed S/S/N three-coil structure IPT system. The circuit model and the theoretical derivation for achieving CC output function and ZPA operation are provided. In Section 3, the three-coil loosely coupled transformer (LCT) is designed, and the detailed system parameter design scheme is provided. Then, the CC output characteristics with ZPA operation is verified by the designed parameters. In addition, the sensitivity of CC output characteristic to changes in compensation capacitance parameters is discussed, and the condition for realizing ZVS is obtained. Section 4 gives the experimental verification of the proposed S/S/N three-coil structure IPT system. Moreover, the proposed IPT system is compared with previous related studies to reflect its advantages. Finally, this paper is concluded in Section 5.

2. Theoretical Analysis

2.1. Overview of the S/S/N Three-Coil Structure IPT System

The overall circuit architecture diagram of the proposed S/S/N three-coil structure IPT system is shown in Figure 1. The operating angular frequency of a high-frequency inverter is represented by ω. L_p, L_s, and L_m are the self-inductances of the transmitting coil, receiving coil, and relay coil, respectively, whereas R_p, R_s, and R_m are the corresponding parasitic resistances. M_{ps}, M_{pm}, and M_{ms} are the mutual inductance between coils. C_p and C_m are the compensation capacitances of L_P and L_m, respectively. The transmitting side of the system comprises a DC voltage source U_d, a high-frequency inverter composed of four MOSFETs, a transmitting coil CL network, and a relay coil CL network; the receiving side comprises the secondary coil L_s, a rectifier D formed by four diodes, and the battery load R_L.

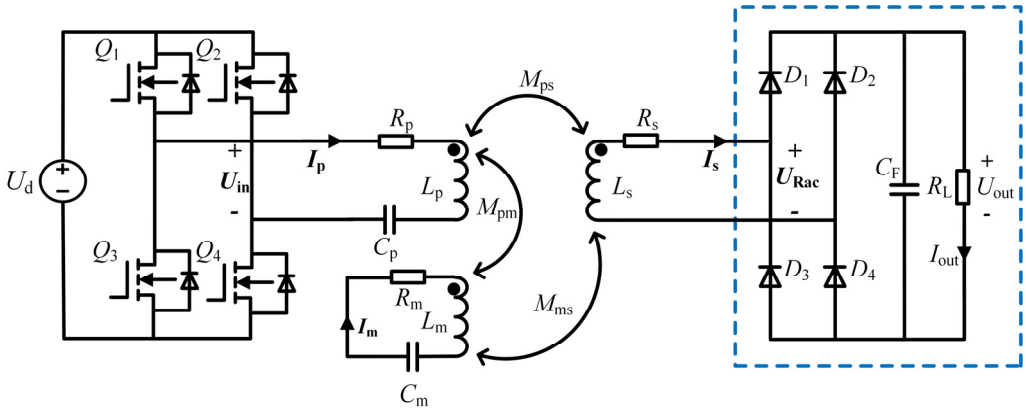

Figure 1. Circuit diagram of the S/S/N three-coil structure IPT system.

Figure 2 is the equivalent circuit diagram of the proposed S/S/N three-coil structure IPT system. As shown in Figure 1, R_{ac} is the equivalent resistance of the part inside the blue box, which can be expressed as.

$$R_{ac} = \frac{8R_L}{\pi^2} \tag{1}$$

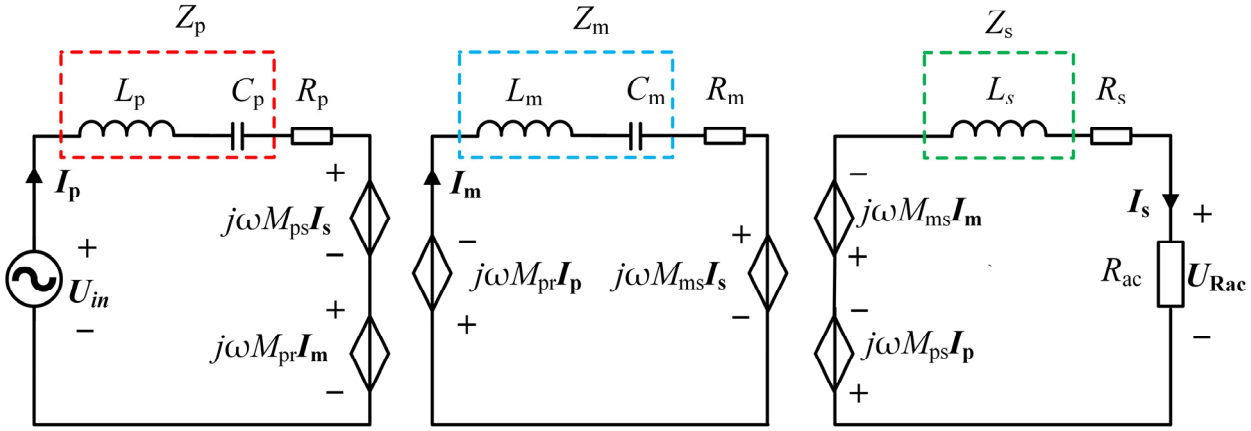

Figure 2. Equivalent circuit diagram of the S/S/N three-coil structure IPT system.

Z_p, Z_m, and Z_s are the impedance of passive components in each coil loop, defined as follows:

$$\begin{cases} Z_p = jX_p = R_p + j\omega L_p + \frac{1}{j\omega C_p} \\ Z_m = jX_m = R_m + j\omega L_m + \frac{1}{j\omega C_m} \\ Z_p = jX_s = R_s + j\omega L_s \end{cases} \tag{2}$$

where X_p, X_m, and X_s are the imaginary parts of Z_p, Z_m, and Z_s, respectively.

U_{in} is input high-frequency AC voltage of the equivalent circuit diagram, U_{in} is the corresponding root mean square (RMS) value and can be expressed as

$$U_{in} = \frac{2\sqrt{2}U_d}{\pi} \tag{3}$$

According to Kirchhoff's voltage law (KVL), the equivalent circuit of the S/S/N three-coil structure IPT system can be obtained as

$$\begin{bmatrix} \boldsymbol{U_{in}} \\ 0 \\ 0 \end{bmatrix} = \begin{bmatrix} Z_p & j\omega M_{ps} & j\omega M_{pm} \\ j\omega M_{ps} & Z_s + R_{ac} & j\omega M_{ms} \\ j\omega M_{pm} & j\omega M_{ms} & Z_m \end{bmatrix} \begin{bmatrix} \boldsymbol{I_p} \\ \boldsymbol{I_s} \\ \boldsymbol{I_m} \end{bmatrix} \tag{4}$$

where $\boldsymbol{I_p}$, $\boldsymbol{I_m}$, and $\boldsymbol{I_s}$ are the current phasors flowing through the transmitting coil, relay coil, and receiving coil, respectively. R_p, R_s, and R_m can be ignored due to relatively small resistances. Based on Equation (4), $\boldsymbol{I_p}$, $\boldsymbol{I_m}$, and $\boldsymbol{I_s}$ can be calculated by

$$\begin{cases} \boldsymbol{I_p} = \frac{(\omega^2 M_{ms}^2 + R_{ac} Z_m + Z_s Z_m)\boldsymbol{U_{in}}}{A + BR_{ac}} \\ \boldsymbol{I_m} = -\frac{(j\omega M_{pm} Z_s + j\omega M_{pm} R_{ac} + \omega^2 M_{ps} M_{ms})\boldsymbol{U_{in}}}{A + BR_{ac}} \\ \boldsymbol{I_s} = -\frac{(j\omega M_{ps} Z_m + \omega^2 M_{pm} M_{ms})\boldsymbol{U_{in}}}{A + BR_{ac}} \end{cases} \tag{5}$$

where the capital letters A and B are expressed as

$$\begin{cases} A = -2j\omega^3 M_{ps} M_{ms} M_{pm} + \omega^2 M_{ps}^2 Z_m + \omega^2 M_{ms}^2 Z_p + \omega^2 M_{pm}^2 Z_s + Z_p Z_s Z_m \\ B = Z_p Z_m + \omega^2 M_{pm}^2 \end{cases} \tag{6}$$

2.2. Analysis of the CC Output Characteristics with ZPA Operation

Based on the above analysis, to achieve the CC output function, the output current I_s should be independent of the equivalent load resistance R_{ac}. As evident from Equation (5), when equation B = 0 holds, the output current I_s is not affected by the variable load resistance, that is

$$Z_p Z_m + \omega^2 M_{pm}^2 = 0 \tag{7}$$

According to Equations (5) and (7), the equivalent input impedance Z_{in} (=$\boldsymbol{U}_{in}/\boldsymbol{I}_P$) is obtained as

$$Z_{in} = \frac{A + BR_{ac}}{\omega^2 M_{ms}^2 + R_{ac} Z_m + Z_m Z_s} \tag{8}$$

To achieve ZPA operation, the imaginary part of Z_{in} should be zero. Based on Equation (8), the following equation should be satisfied.

$$Z_m Z_s + \omega^2 M_{ms}^2 = 0 \tag{9}$$

Then, the constraints on the CC output characteristic with ZPA input can be summed up as

$$\begin{cases} Z_p Z_m + \omega^2 M_{pm}^2 = 0 \\ Z_m Z_s + \omega^2 M_{ms}^2 = 0 \end{cases} \tag{10}$$

Substituting Equation (10) into (5), $\boldsymbol{I_p}$, $\boldsymbol{I_m}$, and $\boldsymbol{I_s}$ can be further simplified as

$$\begin{cases} \boldsymbol{I_p} = -\frac{R_{ac}}{(j\omega M_{ps} - \sqrt{Z_p Z_s})^2}\boldsymbol{U_{in}} \\ \boldsymbol{I_m} = \frac{(Z_s + R_{ac})\sqrt{Z_p Z_m} - j\omega M_{ps}\sqrt{Z_m Z_s}}{Z_m (j\omega M_{ps} - \sqrt{Z_p Z_s})^2}\boldsymbol{U_{in}} \\ \boldsymbol{I_s} = \frac{\boldsymbol{U_{in}}}{j\omega M_{ps} - \sqrt{Z_p Z_s}} \end{cases} \tag{11}$$

Therefore, Z_{in} under the conditions of CC output function and ZPA operation can be simplified as

$$Z_{in} = \frac{(j\omega M_{ps} - \sqrt{Z_p Z_s})^2}{-R_{ac}} = \frac{(\omega M_{ps} - \sqrt{X_p X_s})^2}{R_{ac}} \tag{12}$$

In addition, when conditional Equation (10) is satisfied, the value of the trans-conductance G (defined as the absolute value of the ratio of the output current phasor $\boldsymbol{I_s}$ to the input voltage phasor $\boldsymbol{U_{in}}$) can be obtained and simplified as

$$G = \left| \frac{\boldsymbol{I_s}}{\boldsymbol{U_{in}}} \right| = \left| \frac{1}{j\omega M_{ps} - \sqrt{Z_p Z_s}} \right| \tag{13}$$

Obviously, it can be seen from Equations (12) and (13) that the imaginary part of Z_{in} is nullified, and the output current is independent of R_{ac}. Therefore, CC output function and ZPA input over the full load range can be achieved when Equation (10) is satisfied.

3. Design of the Proposed S/S/N Three-Coil Structure IPT System

3.1. Design the LCT Structure

According to ref. [23], the square coil structure with rounded corners has the combined advantages of the circular coil and square coil, which is selected in this study for coil design. The relay coil is placed coaxially with the transmitting coil, which can effectively reduce the space occupied by the charging device and increase the mutual inductance. In addition, ferrite bars are adopted to improve the magnetic field. Finally, the 3D model of the three-coil LCT built by using the electromagnetic field analysis software Ansoft Maxwell [24] is shown in Figure 3. The specific parameters of LCT are listed in Table 1.

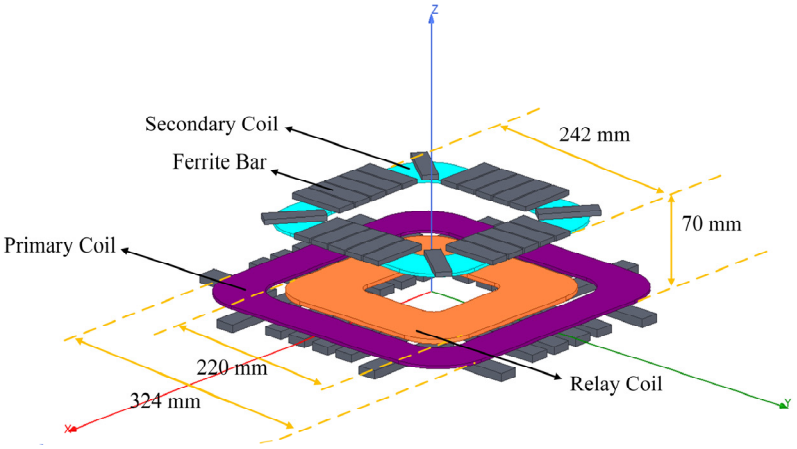

Figure 3. The 3D model of the designed three-coil LCT.

Table 1. Dimension parameters of the designed three-coil LCT.

Parameters	Transmitting Coil	Relay Coil	Receiving Coil
Outer diameter	324 mm	220 mm	242 mm
Internal diameter	240 mm	100 mm	170 mm
Turns of coils (n)	14	15	12
Specifications of Litz wire	400 strands	1000 strands	400 strands
AWG	12	8	12

3.2. Parameter Design

According to the above analysis, the proposed S/S/N three-coil structure IPT system can realize the CC output characteristic with ZPA input when Equation (10) is satisfied. Therefore, substituting Equation (10) into (2), the expressions of compensation capacitances C_p and C_m can be calculated as

$$\begin{cases} C_p = \frac{M_{ms}^2}{\omega^2(L_p M_{ms}^2 - L_s M_{pm}^2)} \\ C_m = \frac{L_s}{\omega^2(L_s L_m - M_{ms}^2)} \end{cases} \quad (14)$$

Once the structure of the LCT is determined, the parameters in the LCT can be calculated by the electromagnetic field analysis software Ansoft Maxwell or measured by an LCR meter. Then, the values of C_p and C_m can be obtained based on (14). The theoretical values of the specific parameters in the proposed system are given in Table 2. Among them, f represents the operating frequency of the system.

Table 2. Theoretical values of the specific parameters in the proposed IPT system.

Parameters	Value	Parameters	Value
f	85 kHz	U_d	60 V
Rated Power	200 W	C_p	47.60 nF
L_p	170.49 μH	C_m	53.70 nF
L_s	86.52 μH	R_p	0.17 Ω
L_m	81.34 μH	R_s	0.09 Ω
M_{ps}	42.69 μH	R_m	0.06 Ω
M_{pm}	39.42 μH	I_{out}	2 A
M_{ms}	37.26 μH		

3.3. Simulation Verification

In order to preliminarily verify the above theoretical analysis, the simulation model of the proposed S/S/N three-coil structure IPT system was established using Matlab software. Substituting the parameters in Table 2 into the established simulation model, the graphs of the output current and input impedance angle under different load conditions were drawn, as shown in Figure 4. It can be clearly seen that the designed S/S/N three-coil structure IPT system can realize CC output characteristics with ZPA input at a frequency of 85 kHz, which verifies the feasibility of the proposed system.

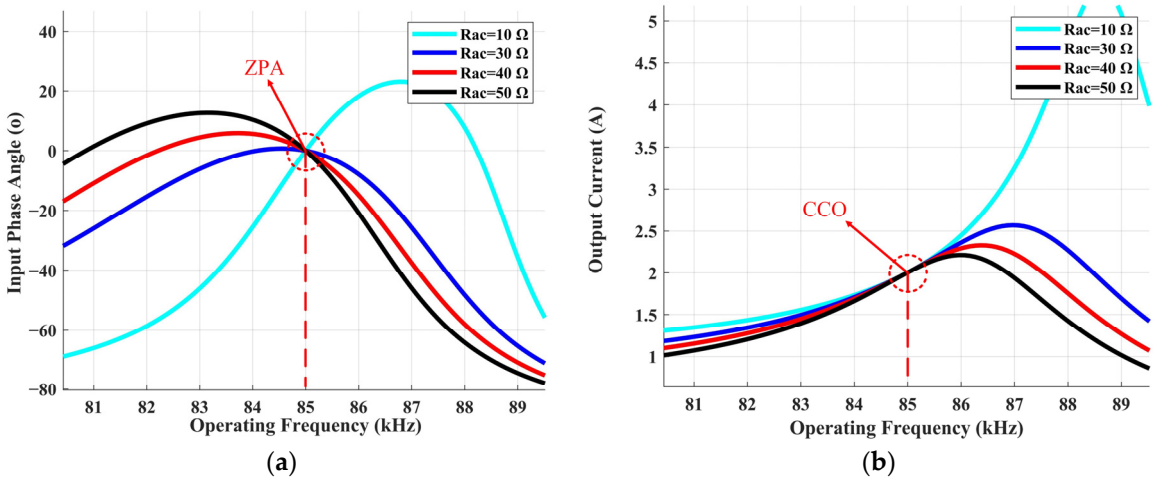

(**a**) (**b**)

Figure 4. Curves of the output current and input impedance angle under different load conditions: (**a**) Input Phase Angle; (**b**) Output Current.

3.4. Verification of ZVS Operation

Since there are no–negligible parasitic capacitances in the four MOSFETs, the input impedance angle of the system should be slightly inductive to obtain the ZVS operation for improving the efficiency of high-frequency inverter. The input impedance angle is defined as

$$\theta_{in} = \frac{180}{\pi} \tan^{-1} \frac{\mathrm{Im}(Z_{in})}{\mathrm{Re}(Z_{in})} \tag{15}$$

According to Equations (8) and (15), the input impedance angle of the proposed system is further expressed as

$$\theta_{in} = \arctan\left(\frac{X_m R_{ac}}{X_s X_m - \omega^2 M_{ms}^2}\right) \tag{16}$$

Once the LCT is established, the self-inductances and mutual inductances of the system are determined. According to Equation (16), the input impedance angle can be changed by adjusting the value of the compensation capacitors. Figure 5 shows the relationship between the input impedance angle and the compensation capacitances C_p and C_m under different load conditions.

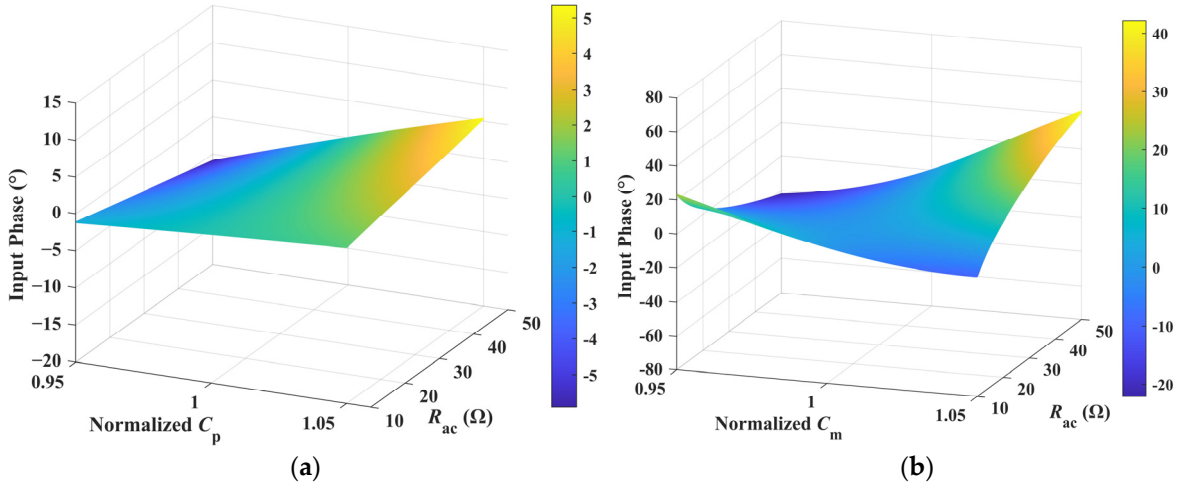

Figure 5. Input impedance angle versus R_{ac} and normalized capacitances: (**a**) C_p; (**b**) C_m.

Obviously, a slight increase in the values of C_p and C_m contributes to a positive input impedance angle. However, the values of C_p and C_m are limited by the preset CC output function. It is therefore necessary to compare the sensitivity to the changes in C_p and C_m to the CC output function. Specifically, the capacitance parameters are normalized, and R_{ac} is increased from 10 to 50 Ω. The system output currents versus the normalized parameters of C_p and C_m under different load conditions are shown in Figure 6.

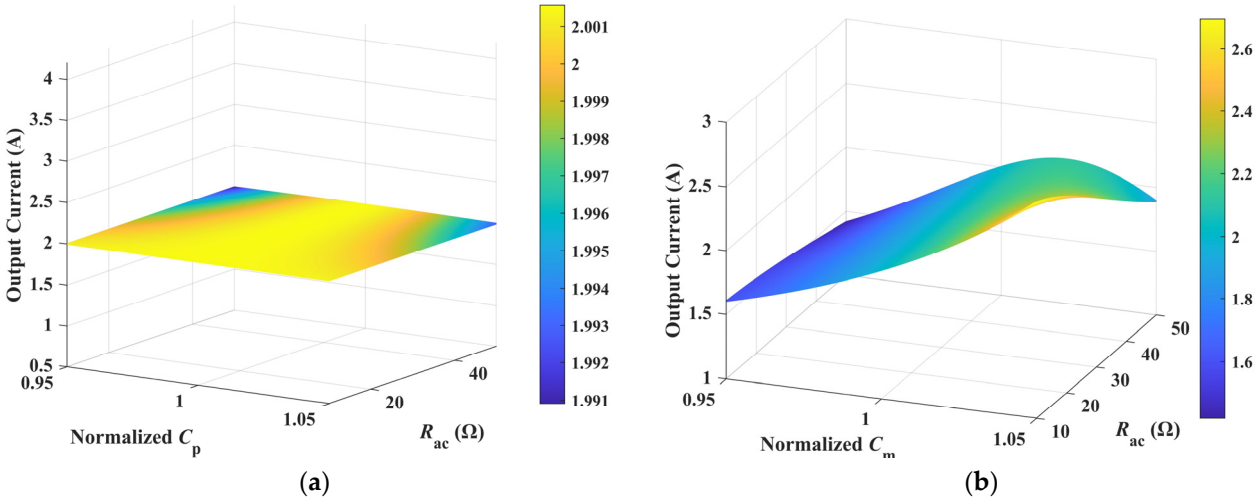

Figure 6. Output current versus R_{ac} and normalized capacitances: (**a**) C_p; (**b**) C_m.

According to Figure 6, the change in the normalized C_m has a significant impact on the output current. Therefore, the CC output characteristic is highly sensitive to C_m. However, the change in the normalized C_p basically does not affect the value of the output current. Therefore, a slight increment of C_p should be selected to achieve the ZVS operation.

4. Experimental Verification

To verify the correctness and practicability of the above theory, an experimental prototype was fabricated, as shown in Figure 7. The hardware of the experimental prototype is made up of a DC voltage source, compensation capacitor C_p, compensation capacitor C_m, LCT, high-frequency inverter, rectifier, load, and an oscilloscope, which are numbered 1 to 8, respectively.

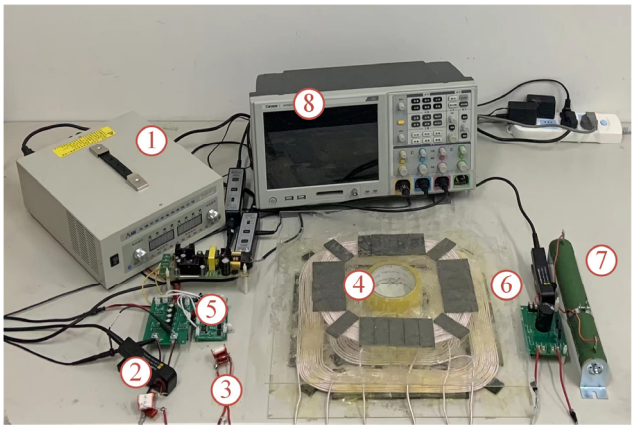

Figure 7. Experimental setup of the proposed three-coil structure IPT system.

The three-coil LCT, which is set according to the parameters listed in Table 1, is displayed in Figure 8. The measured values of the specific parameters in the proposed IPT system are given in Table 3, which slightly deviates from the theoretical values in Table 2. First, the implementation of the CC output function with ZPA input is verified under different load conditions. Figure 9a–c show the experimental waveforms of $\boldsymbol{U_{in}}$, $\boldsymbol{I_p}$, and I_{out} under the ZPA operation condition at load resistances of 10 Ω, 20 Ω, and 30 Ω, respectively. It can be seen intuitively that $\boldsymbol{U_{in}}$ and $\boldsymbol{I_p}$ are always in phase, which means that the proposed system can realize the ZPA operation. Moreover, the output current remains constant at 2A under different load conditions, which verifies the excellent CC output characteristic of the proposed system.

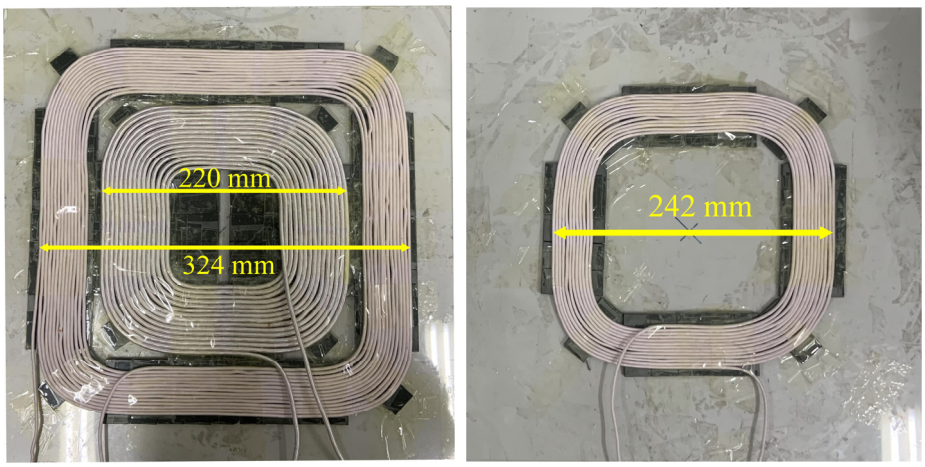

(**a**) (**b**)

Figure 8. Experimental prototype of charging pads: (**a**) transmitting pad; (**b**) receiving pad.

Table 3. Measured values of the specific parameters in the proposed IPT system.

Parameters	Value	Parameters	Value
f	85 kHz	U_d	60 V
Rated Power	200 W	C_{p_ZPA}	42.89 nF
L_p	171.98 μH	C_m	53.64 nF
L_s	87.42 μH	C_{p_ZVS}	47.18 nF
L_m	82.05 μH	R_p	0.18 Ω
M_{ps}	43.90 μH	R_s	0.09 Ω
M_{pm}	38.81 μH	R_m	0.06 Ω
M_{ms}	38.20 μH	I_{out}	2A

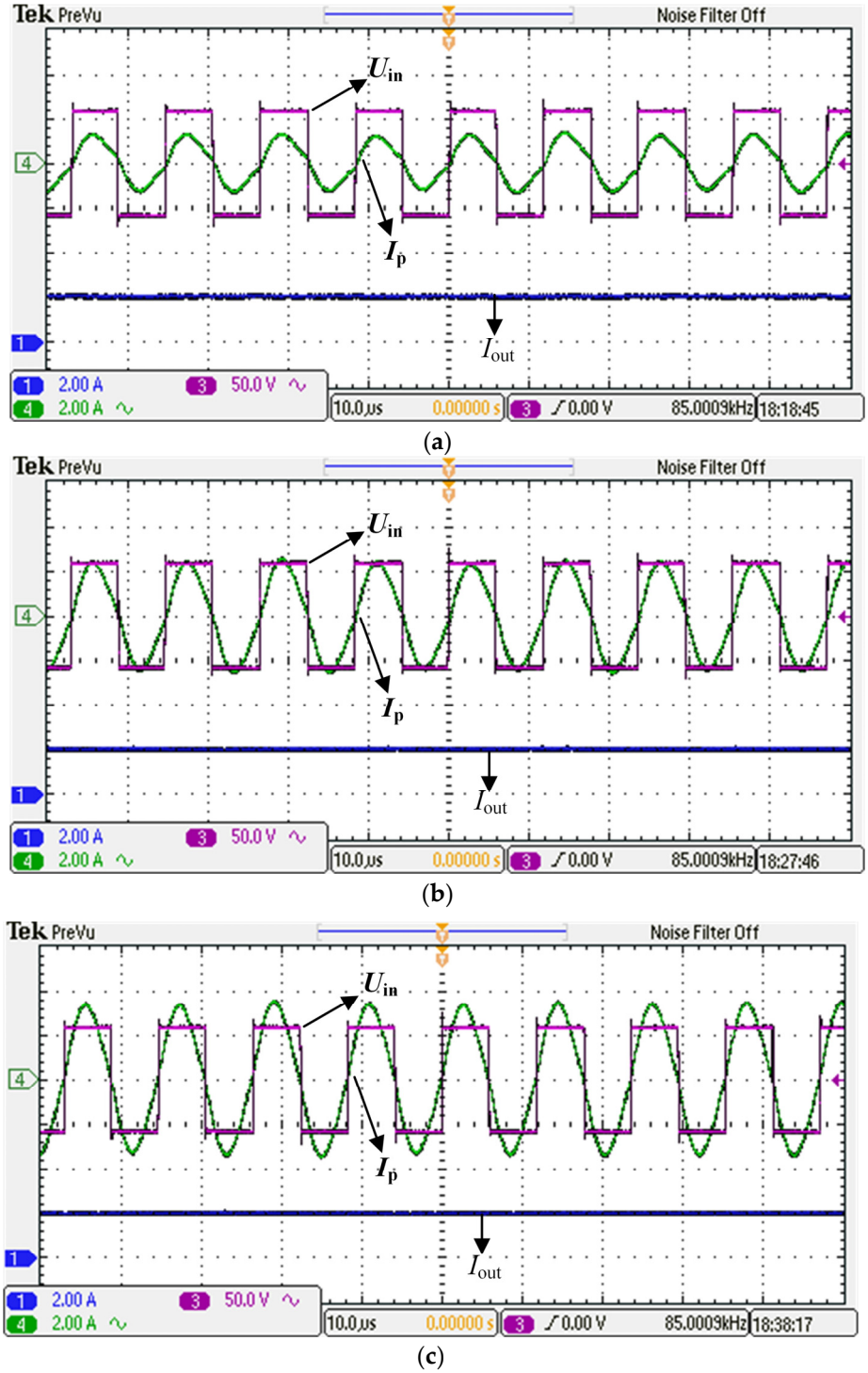

Figure 9. Experimental waveforms of the IPT system when ZPA condition is employed and resistive load equals to (**a**) 10 Ω; (**b**) 20 Ω; (**c**) 30 Ω.

Then, the compensation capacitance C_{p_zpa} is adjusted to C_{p_zvs} to verify the ZVS operation. Figure 10a–c display the waveforms of $\boldsymbol{U_{in}}$, $\boldsymbol{I_p}$, and I_{out} under the ZVS operation condition when the load resistances are set at 10, 20, and 30 Ω, respectively. It is clear that $\boldsymbol{I_p}$ has a certain lagging phase angle towards $\boldsymbol{U_{in}}$, which means the realization of the ZVS operation. In addition, the output current I_{out} is always kept at 2A, which means that the realization of ZVS operation does not affect the CC output characteristic of the proposed system.

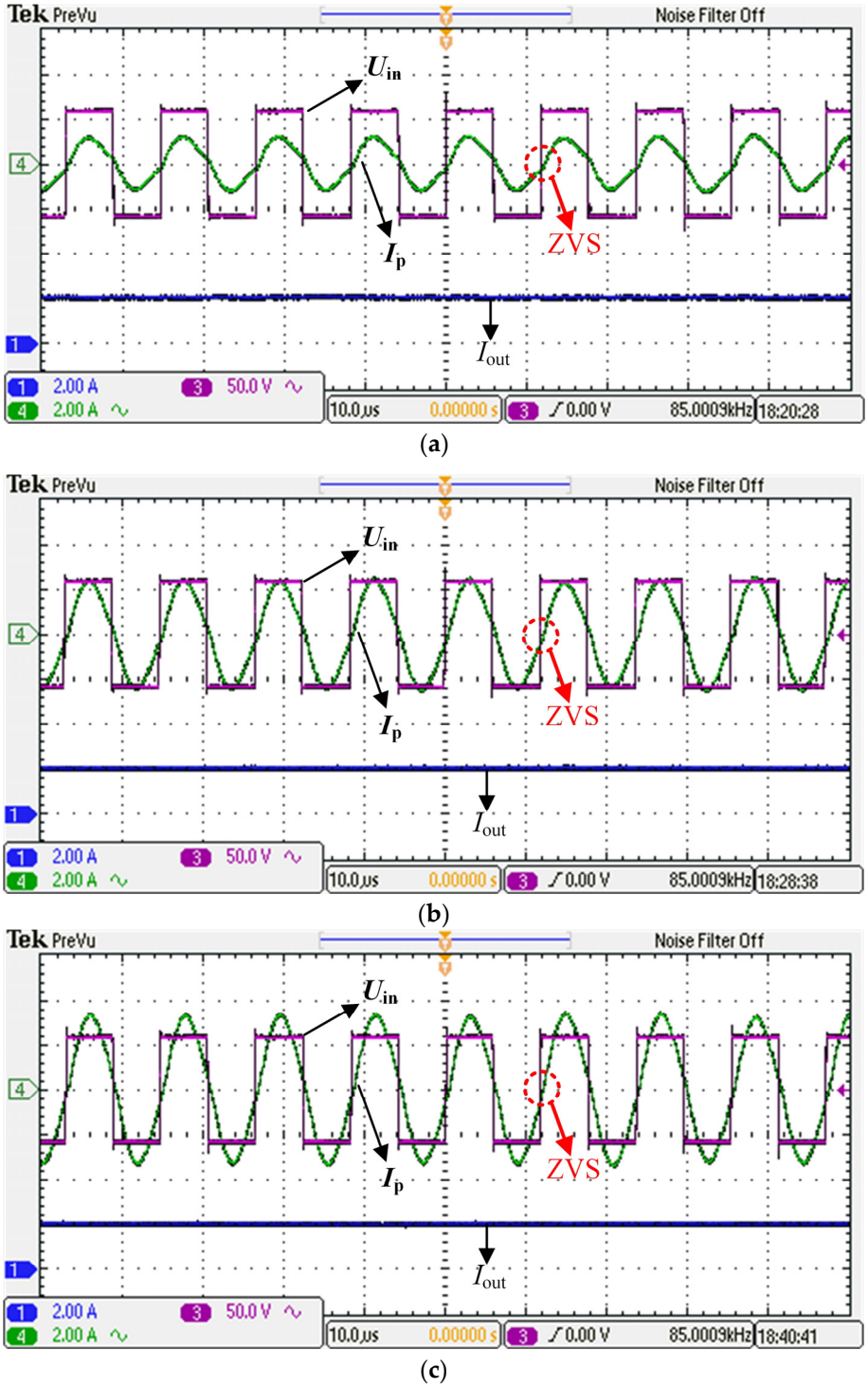

Figure 10. Experimental waveforms of the IPT system when ZVS condition is employed and resistive load equals to (**a**) 10 Ω; (**b**) 20 Ω; (**c**) 30 Ω.

Figure 11 shows the system efficiency profile against varying load resistances throughout the whole charging process. It can be observed that the system efficiency first increases from 86.23% to the peak value of 92.12%, then gradually decreases to 88.54% until the end of the charging. In addition, the efficiency of this study is compared with the S/S/S three-coil structure IPT system with capacitors in the receiver. The parameters of the LCT of the S/S/S three-coil structure IPT system are consistent with the LCT parameters designed in this study, and the charging voltage and operating frequency are set to 60 V and 85 kHz,

respectively. Moreover, the values of the compensation capacitors for the S/S/S three-coil structure IPT system are listed in Table 4. It can be seen from Figure 11 that the energy transfer efficiency of the proposed S/S/N three-coil structure IPT system is comparable to that of the S/S/S three-coil structure IPT system. However, the proposed system has structural advantages over the S/S/S three-coil structure IPT system. That is, there are no compensation components on the receiving side of the proposed system. A low-cost, lightweight, and compact receiver is ensured, which is crucial in special wireless charging applications, for example, implantable medical devices (IMDs) and unmanned aerial vehicles (UAVs) that have strict requirements on volume and weight, and others.

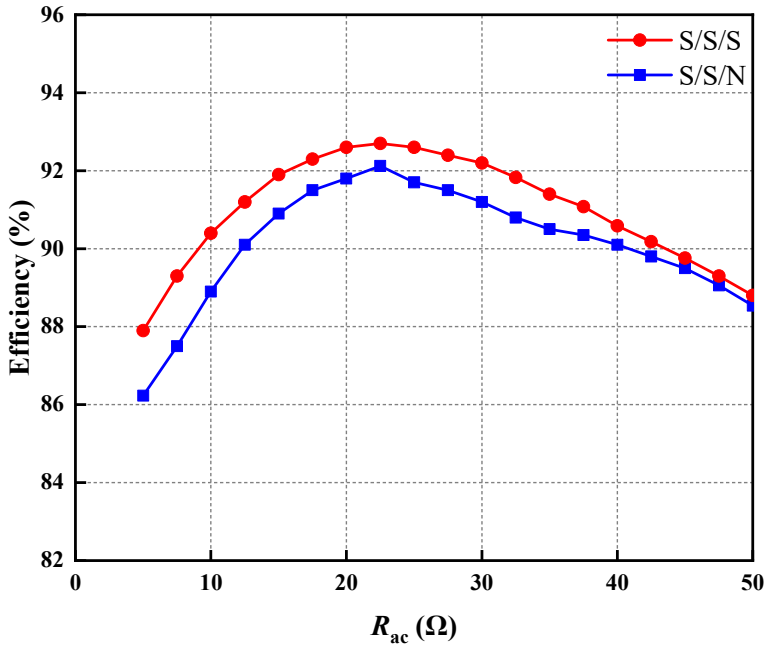

Figure 11. Efficiency of the proposed S/S/N three-coil structure IPT system in the whole charging process and comparison with the efficiency of the S/S/S three-coil structure IPT system.

Table 4. Compensation capacitors' parameters of the S/S/S-compensated three-coil structure IPT system adopting the LCT parameters designed in this study.

Parameters	Designed Value	Measured Value
C_p	19.717 nF	19.609 nF
C_m	11.548 nF	11.565 nF
C_s	37.377 nF	37.289 nF

To further specify the superiority of the CC-Type IPT system based on the S/S/N three-coil structure, several other CC-Type IPT systems are introduced for performance comparison. The detailed comparison results are provided in Table 5. From Table 5, compared to the CC-Type IPT systems proposed in [16–22], the proposed S/S/N three-coil IPT system does not have any compensation components on the receiving side, so a low-cost, lightweight and compact receiver can be further guaranteed.

Table 5. Comparison of this work with previous similar works.

Proposed	[16]	[17]	[18]	[19]	[20]	[21]	[22]	This Work
Resonant tank	LC-CC	LCL/P	S/S/P	LCC-LCC	LC-CL	LC/S	SS	S/S/N
Number of coils	2	2	3	2	2	2	2	3
Number of compensation components in transmitter	2	3	2	3	2	2	1	2
Number of compensation components in receiver	2	1	1	3	2	1	1	0
Without compensation components and filter inductor in receiver	no	no	no	no	no	no	no	yes
Low-cost and compact receiver	no	no	no	no	no	no	no	yes

5. Conclusions

This study proposed a CC-type IPT system based on an S/S/N three-coil structure and the corresponding parameter tuning method. The CC output function with ZPA input can be realized through flexible parameter design. In addition, the ZVS operation without affecting the CC output function of the proposed system can be achieved by slightly increasing the value of the compensation capacitor C_p on the transmitting coil loop. It is worth mentioning that the proposed S/S/N three-coil structure IPT system does not require additional compensation components and a bulky filter inductor on the receiver. Therefore, a low-cost, lightweight, and compact receiver of the IPT system can be achieved. Compared with previous related studies, the structural and economic properties of the proposed S/S/N three-coil structure IPT system have been improved. Thus, the proposed S/S/N three-coil structure IPT system has potential application value.

Author Contributions: Conceptualization, L.Y. and S.S.; methodology, L.Y.; software, S.S.; validation, L.Y., S.S., H.W. and S.J.; formal analysis, L.Z.; investigation, L.Y. and S.S.; resources, L.Y.; data curation, S.S.; writing—original draft preparation, S.S.; writing—review and editing, L.Y.; visualization, H.W.; supervision, L.Y.; funding acquisition, L.Y. All authors have read and agreed to the published version of the manuscript.

Funding: This research was funded in part by Natural Science Foundation of Henan Province of China under Grant 212300410173, in part by the Key Research Program of Higher Education of Henan under Grant 23A470007, and in part by Doctor Initiative Foundation of Henan Normal University under Grant 20210244 and 20210269.

Data Availability Statement: Not applicable.

Conflicts of Interest: The authors declare no conflict of interest.

References

1. Zhang, Z.; Pang, H.; Georgiadis, A.; Cecati, C. Wireless power transfer—An overview. *IEEE Trans. Ind. Electron.* **2018**, *66*, 1044–1058. [CrossRef]
2. Yang, L.; Shi, Y.; Wang, M.; Ren, L. Constant Voltage Charging and Maximum Efficiency Tracking for WPT Systems Employing Dual-Side Control Scheme. *IEEE J. Emerg. Sel. Top. Power Electron.* **2021**, *10*, 945–955. [CrossRef]
3. Yao, Y.; Gao, S.; Mai, J.; Liu, X.; Zhang, X.; Xu, D. A Novel Misalignment Tolerant Magnetic Coupler for Electric Vehicle Wireless Charging. *IEEE J. Emerg. Sel. Top. Ind. Electron.* **2021**, *3*, 219–229. [CrossRef]
4. Li, Z.; Li, J.; Li, S.; Yu, Y.; Yi, J. Design and Optimization of Asymmetric and Reverse Series Coil Structure for Obtaining Quasi-Constant Mutual Inductance in Dynamic Wireless Charging System for Electric Vehicles. *IEEE Trans. Veh. Technol.* **2021**, *71*, 2560–2572. [CrossRef]
5. Hui, S.Y. Planar Wireless Charging Technology for Portable Electronic Products and Qi. *Proc. IEEE* **2013**, *101*, 1290–1301. [CrossRef]
6. Feng, J.; Li, Q.; Lee, F.C.; Fu, M. Transmitter Coils Design for Free-Positioning Omnidirectional Wireless Power Transfer System. *IEEE Trans. Ind. Inform.* **2019**, *15*, 4656–4664. [CrossRef]
7. Agarwal, K.; Jegadeesan, R.; Guo, Y.-X.; Thakor, N.V. Wireless Power Transfer Strategies for Implantable Bioelectronics. *IEEE Rev. Biomed. Eng.* **2017**, *10*, 136–161. [CrossRef]

8. Xiao, C.; Cheng, D.; Wei, K. An LCC-C Compensated Wireless Charging System for Implantable Cardiac Pacemakers: Theory, Experiment, and Safety Evaluation. *IEEE Trans. Power Electron.* **2018**, *33*, 4894–4905. [CrossRef]
9. Cai, C.; Wang, J.; Zhang, F.; Liu, X.; Zhang, P.; Zhou, Y.-G. A Multichannel Wireless UAV Charging System With Compact Receivers for Improving Transmission Stability and Capacity. *IEEE Syst. J.* **2021**, *16*, 997–1008. [CrossRef]
10. Wang, J.; Chen, R.; Cai, C.; Zhang, J.; Wang, C. An Onboard Magnetic Integration Based WPT System for UAV Misalignment-Tolerant Charging with Constant Current Output. *IEEE Trans. Transp. Electrif.* **2022**, 1. [CrossRef]
11. Chen, Y.; Yang, N.; Li, Q.; He, Z.; Mai, R. New parameter tuning method for LCC/LCC compensated IPT system with constant voltage output based on LC resonance principles. *IET Power Electron.* **2019**, *12*, 2466–2474. [CrossRef]
12. Jia, H.; Qianhong, C.; Siu-Chung, W.; Tse, C.K.; Xinbo, R. Analysis and Control of Series/Series-Parallel Compensated Resonant Converter for Contactless Power Transfer. *IEEE J. Emerg. Sel. Top. Power Electron.* **2015**, *3*, 124–136. [CrossRef]
13. Wang, Y.; Yao, Y.; Liu, X.; Xu, D. S/CLC Compensation Topology Analysis and Circular Coil Design for Wireless Power Transfer. *IEEE Trans. Transp. Electrif.* **2017**, *3*, 496–507. [CrossRef]
14. Li, Y.; Hu, J.; Li, X.; Chen, F.; Xu, Q.; Mai, R.; He, Z. Analysis, Design, and Experimental Verification of a Mixed High-Order Compensations-Based WPT System with Constant Current Outputs for Driving Multistring LEDs. *IEEE Trans. Ind. Electron.* **2019**, *67*, 203–213. [CrossRef]
15. Li, Y.; Hu, J.; Li, X.; Wang, H.; Cheng, K.W.E. Cost-Effective and Compact Multistring LED Driver Based on a Three-Coil Wireless Power Transfer System. *IEEE Trans. Power Electron.* **2019**, *34*, 7156–7160. [CrossRef]
16. Qu, X.; Chu, H.; Huang, Z.; Wong, S.-C.; Tse, C.K.; Mi, C.C.; Chen, X. Wide Design Range of Constant Output Current Using Double-Sided LC Compensation Circuits for Inductive-Power-Transfer Applications. *IEEE Trans. Power Electron.* **2018**, *34*, 2364–2374. [CrossRef]
17. Yao, Y.; Liu, X.; Wang, Y.; Xu, D. Modified parameter tuning method for LCL/P compensation topology featured with load-independent and LCT-unconstrained output current. *IET Power Electron.* **2018**, *11*, 1483–1491. [CrossRef]
18. Yang, L.; Ren, L.; Shi, Y.; Wang, M.; Geng, Z. Analysis and Design of a S/S/P-Compensated Three-coil Structure WPT System With Constant Current and Constant Voltage Output. *IEEE J. Emerg. Sel. Top. Power Electron.* **2022**, 1. [CrossRef]
19. Vu, V.-B.; Tran, D.-H.; Choi, W. Implementation of the Constant Current and Constant Voltage Charge of Inductive Power Transfer Systems With the Double-Sided LCC Compensation Topology for Electric Vehicle Battery Charge Applications. *IEEE Trans. Power Electron.* **2017**, *33*, 7398–7410. [CrossRef]
20. Yao, Y.; Liu, X.; Wang, Y.; Xu, D. LC/CL compensation topology and efficiency-based optimisation method for wireless power transfer. *IET Power Electron.* **2018**, *11*, 1029–1037. [CrossRef]
21. Wang, Y.; Yao, Y.; Liu, X.; Xu, D.; Cai, L. An LC/S Compensation Topology and Coil Design Technique for Wireless Power Transfer. *IEEE Trans. Power Electron.* **2017**, *33*, 2007–2025. [CrossRef]
22. Qu, X.; Han, H.; Wong, S.-C.; Tse, C.K.; Chen, W. Hybrid IPT Topologies With Constant Current or Constant Voltage Output for Battery Charging Applications. *IEEE Trans. Power Electron.* **2015**, *30*, 6329–6337. [CrossRef]
23. Cai, C.; Wang, J.; Fang, Z.; Zhang, P.; Hu, M.; Zhang, J.; Li, L.; Lin, Z. Design and Optimization of Load-Independent Magnetic Resonant Wireless Charging System for Electric Vehicles. *IEEE Access* **2018**, *6*, 17264–17274. [CrossRef]
24. John Swanson. *Ansoft Maxwell*, version 16.0; Ansys, Inc.: Canonsburg, PA, USA, 2016.